ELSEVIER

Journal of Photochemistry and Photobiology A: Chemistry 153 (2002) 211–219

Journal of Photochemistry and Photobiology A:Chemistry

www.elsevier.com/locate/jphotochem

Bactericidal and photocatalytic activities of TiO_2 thin films prepared by sol–gel and reverse micelle methods

Jimmy C. Yu [a,*], Hung Yuk Tang [a], Jiaguo Yu [a], H.C. Chan [b], Lizhi Zhang [a], Yinde Xie [a], H. Wang [c], S.P. Wong [c]

[a] *Department of Chemistry, The Chinese University of Hong Kong, Shatin, New Territories, Hong Kong, China*
[b] *Department of Physiology, The Chinese University of Hong Kong, Shatin, New Territories, Hong Kong, China*
[c] *Department of Electronic Engineering and Materials Science & Technology Research Centre, The Chinese University of Hong Kong, Shatin, New Territories, Hong Kong, China*

Received 5 February 2002; received in revised form 12 June 2002; accepted 10 July 2002

Abstract

The present study investigated bactericidal and photocatalytic activities of transparent anatase TiO_2 thin films on soda-lime glass prepared by using reverse micelle and sol–gel methods. Both films exhibited significant bactericidal activity towards three strains of *Escherichia coli*, namely DH5α, JM109 and XL1 Blue MRF'. The TiO_2 films were characterized by X-ray photoelectron spectroscopy (XPS), atomic force microscopy (AFM), X-ray diffraction (XRD), and UV-Vis spectrometry. Results of photocatalytic activity measurements suggest that the TiO_2 film prepared by the reverse micelle method is a better photocatalyst than that prepared by sol–gel method in gaseous phase oxidation but their activities in aqueous phase are about the same.

Keywords: TiO_2 thin films; Sol–gel method; Reverse micelle method; *E. coli*; Bactericidal activity; Rhodamine B

1. Introduction

Common disinfection methods such as chlorination, ozonation and UV irradiation have limitations. For chlorination and ozonation, trihalomethanes (THM) and other carcinogenic disinfection by-products (DBP) maybe generated. For UV disinfection, the process may not be effective enough as some of the bacteria may have mutated and developed resistance towards UV light [1].

Since the discovery of the photocatalytic splitting of water on titanium dioxide (TiO_2) electrode in 1972 by Fujishima and Honda [2], this semiconductor has been extensively investigated. Many studies have focused on the degradation of hazardous and toxic organic compounds such as trichloroethylene (TCE) [3–9] and aromatics [10–14]. Since the mechanism of photodegradation by TiO_2 involves the generation of oxidizing species [15–19], it is believed that UV-irradiated TiO_2 can be used to kill bacteria by its oxidizing power. In 1985, Matsunaga et al. [20] reported that *Lactobacillus acidophilus*, *Saccharomyces cerevisiae* and *Escherichia coli* could be killed by contact with a TiO_2–Pt catalyst under near-UV illumination for 60–120 min. A few years later, the same group constructed a photochemical device and applied the immobilized TiO_2 to kill *E. coli* specifically [21]. Since then, many studies on the bactericidal effect of TiO_2 have been reported [22–29]. Most of these studies used the conventional powder photocatalyst, commonly the Degussa P25. These photocatalyst powders, however, are difficult to separate and recover after disinfection. Immobilization of TiO_2 on an inert substrate to form a bactericidal surface seems to be a practical solution [21,30–34].

In this paper, we describe the preparation of two types of transparent TiO_2 thin films using sol–gel [35,36] and reverse micelle [37–39] methods. These thin films were characterized by X-ray photoelectron spectroscopy (XPS), atomic force microscopy (AFM), X-ray diffraction (XRD), and UV-Vis spectrophotometry. The bactericidal activities of the samples were evaluated by the inactivation of three strains of *E. coli*, namely DH5α, JM109 and XL1 Blue MRF', based on the decrease in the colony of *E. coli* formed on agar plates. The photocatalytic activities of the thin films were also measured by the degradation of acetone in gaseous phase and Rhodamine B (RB) in aqueous phase.

We have found that the bactericidal effects of the two types of TiO_2 films are dependent on the structural features

* Corresponding author. Tel.: +852-2609-6268; fax: +852-2603-5057.
E-mail address: jimyu@cuhk.edu.hk (J.C. Yu).

1010-6030/02/$ – see front matter
PII: S1010-6030(02)00275-7

of titania, the strains of *E. coli* and the cell concentration. Our photocatalytic activity measurements show that the reverse micelle (RM-TiO_2) film is more effective than the sol–gel (SG-TiO_2) film in the degradation of gaseous acetone. However, the two are just as effective in the aqueous phase degradation of RB. An explanation is given based on the film structure and molecular/species size.

2. Experimental details

2.1. Materials

Titanium isopropoxide was supplied by Acros; triethanolamine and Triton X-100 were supplied by BDH; phosphate buffer solution (PBS) was supplied by Aldrich; agar was supplied by Sigma; and Luria–Bertani (LB) broth was supplied by USB. All chemicals were used as received. Millipore water was used in all experiments.

2.2. Preparation of TiO_2 thin films

For the preparation of SG-TiO_2 thin films, a precursor solution was used [35,36]. Titanium isopropoxide and triethanolamine were dissolved in absolute ethanol and stirred vigorously for 1 h at room temperature. A mixture of water and ethanol was then added in drops to the solution with a dropper under stirring. The resultant alkoxide solution was kept stirring at room temperature for hydrolysis. The resulting TiO_2 sol can be used after 2 h. The molar ratio of the reactants was as follows: $Ti(OC_3H_7)_4$:C_2H_5OH:H_2O:$N(C_2H_4OH)_3$ = 1:26.5:1:1. Soda-lime glass (75 mm × 25 mm × 1.5 mm) was used as the substrate for coating the TiO_2 thin films by dip-coating method. The withdrawal speed was 4 mm s^{-1}. The glass-coated with TiO_2 gel films was calcined in air at a rate of 10 °C min^{-1} up to 500 °C and was left in the furnace at 500 °C for 1 h.

RM-TiO_2 thin films were prepared in a similar way, but the composition of the precursor solution was different [37,38]. Triton X-100 and water were dissolved in 100 ml cyclohexane and stirred vigorously for half-an-hour at room temperature. Titanium isopropoxide was then added to the reaction mixture and stirred for 2 h. The concentration of Triton X-100, titanium isopropoxide and water was 0.2, 0.5 and 0.4 M, respectively. The glass-coated with TiO_2 gel films was calcined in air at a rate of 3 °C min^{-1} up to 500 °C and was left in the furnace at 500 °C for 1 h.

2.3. Culture of microorganisms

Cultures of *E. coli* cells were grown aerobically in 30 ml of LB broth at 37 °C on a rotary shaker (170 rpm) for 18 h. *E. coli* cells were harvested by centrifugation at 6000 × *g* (4 °C) for 5 min, washed and resuspended in 5 ml PBS. Serial dilution of the *E. coli*-containing stock solution with PBS was performed to yield starting concentrations of 10^4, 10^5 and 10^6 colony forming units (CFU) ml^{-1}. The CFUs were determined by spreading appropriate dilutions on duplicate LB agar plates and incubated for 24 h at 37 °C, after which the number of colonies on the plates were counted. All materials were autoclaved at 121 °C for 20 min to ensure sterility.

2.4. Bactericidal activity measurements

An amount of 1 ml of the *E. coli* cell suspension with appropriate CFU was pipetted onto the TiO_2-coated glass. The glass was illuminated by a 15 W long wavelength UV lamp (Vilber-Lourmat, T-15L) positioned 4 cm above the glass. The light intensity at the TiO_2 surface was measured to be 0.63 mW cm^{-2} at the sample position. This was determined by using a UV meter with the peak intensity at 365 nm (model UVX digital radiometer; UVP, San Gabriel, CA).

An amount of 20 or 40 ml aliquots of serially diluted suspensions were plated on duplicate LB agar plates at 10 min intervals. The plates were then incubated at 37 °C for 24 h and the numbers of colonies on the plates were counted.

2.5. Photocatalytic activity to degrade acetone in gas phase

The measurement of photocatalytic activity of the two types of TiO_2 films in the oxidation of acetone in air was performed at ambient temperature using a 7L reactor. Ten pieces of the TiO_2-coated glass were put inside the reactor and then a small amount of acetone was injected. A photoionization detector (MiniRAE Plus Professional PID) monitored the concentration of acetone in the reactor. The acetone vapor was allowed to reach adsorption equilibrium with the photocatalyst in reactor prior to an experiment. The initial concentration of acetone after reaching adsorption equilibrium was 400 ppm. The acetone concentration remained constant until the reactor was illuminated by a 15 W 365 nm UV lamp (Vilber-Lourmat, T-15L).

A nondispersive infrared (NDIR) monitor (Metrosonics aq511) was used to determine the concentration of carbon dioxide in the reactor. During the experiment, the concentration of carbon dioxide increased with decreasing concentration of acetone in the reactor, and a near 3:1 ratio of carbon dioxide formation to acetone degradation was observed. Each reaction lasted for 60 min.

2.6. Photocatalytic activity to degrade RB in aqueous phase

RB aqueous solution (initial concentration = 4×10^{-6} mol dm^{-3}) was prepared and 10 ml of the dye solution was pipetted onto a glass Petri dish that was either empty or contained one piece of the TiO_2-coated glass. A 15 W 365 nm UV lamp (Vilber-Lourmat, T-15L) was used as the light source and it was put 1 cm above the dye solution.

The photocatalytic decomposition of RB was monitored by the decrease of the absorbance at wavelength of 554 nm measured by a UV-Vis spectrophotometer (Cary 100Scan Spectrophotometer, Varian, USA).

2.7. Characterization

XPS measurements were performed on a PHI Quantum 2000 XPS System with a monochromatic Al Kα source and a charge neutralizer; all the binding energies were referenced to the C 1s peak at 284.8 eV of the surface adventitious carbon.

UV-Vis spectra of films were obtained using a UV-Vis spectrophotometer (Cary 100Scan Spectrophotometer, Varian, USA) The film thickness was measured using surface profiler (Alpha-step 500).

AFM (Nano Scope 3a, Digital Instrument, Santa Barbara, CA) was used to evaluate the surface roughness and morphologies of the TiO_2 thin films.

The main phase present was identified and the crystallite size of the TiO_2 thin films was determined by XRD patterns, which were obtained on a Siemens D5005 X-ray diffractometer using Cu Kα radiation at a scan speed of 0.400 s per step with an increment of 0.06° per step. The accelerating voltage and the applied current were 40 kV and 40 mA, respectively. The crystallite size was calculated from X-ray line broadening analysis by Scherrer formula.

3. Results and discussion

3.1. Bactericidal activity

Since the UV source is long wavelength UV and the three strains of *E. coli* that we studied possessed the *recA* gene, which is known to be UV resistant [1,40], bacterial inactivation by UV light alone in the control experiment (glass without any coating of TiO_2) does not occur in our experimental setup. Also, TiO_2 put in the dark does not have any bactericidal effect. The bacterial inactivation occurs with UV irradiated SG- and RM-TiO_2 thin films.

For the strain of *E. coli* DH5α at the cell concentration of 10^4, 10^5 and 10^6 CFU ml^{-1}, the survival percentage of the cell on the two types of TiO_2-coated glass reached near-zero levels after 50 min irradiation. For the cell concentration of 10^6 CFU ml^{-1} (Fig. 1a), the bacterial survival percentage ranged between 80 and 100% for the first 30 min, which then dropped to 30% at 40 min and finally reached <10% at 50 min of UV irradiation. A similar trend appeared at cell concentrations of 10^5 CFU ml^{-1} (Fig. 1b). However, the bacterial survival percentage only stayed high for the first 20 min, after which it started to drop. It reached 40% and <10% at 30 and 40 min of UV irradiation, respectively. The bactericidal process was virtually completed after 50 min. For even lower cell concentrations of 10^4 CFU ml^{-1} (Fig. 1c), the cell numbers started to drop

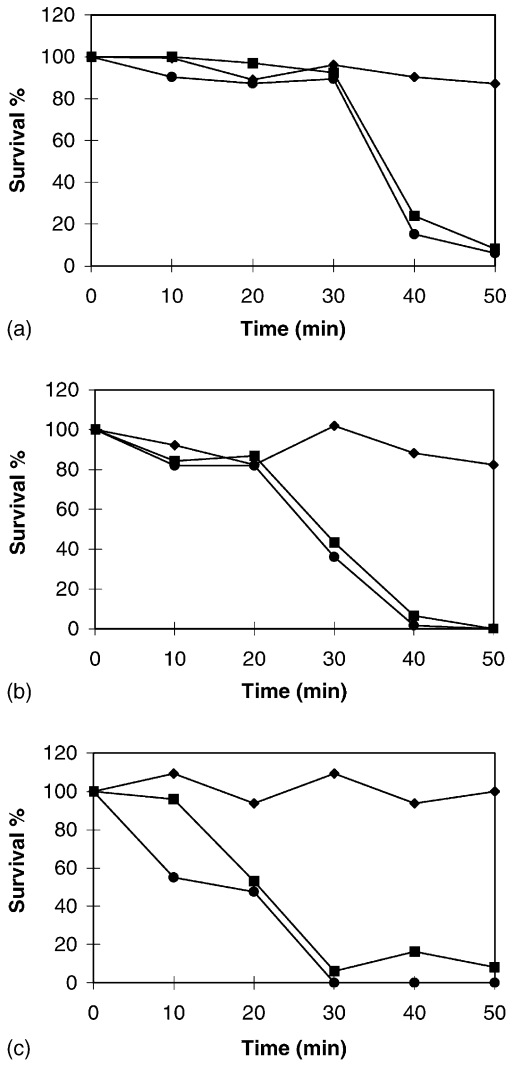

Fig. 1. Effect of SG- and RM-TiO_2 thin films on DH5α survival as a function of time. Initial concentration: (a) 10^6 CFU ml^{-1}; (b) 10^5 CFU ml^{-1}; (c) 10^4 CFU ml^{-1}. Glass (◆); SG-TiO_2 (■); RM-TiO_2 (●).

at the beginning and reached <10% after 30 min of UV illumination.

From the above results, it can be concluded that the time for inactivating the cell number of DH5α is dependent on the initial cell concentration. The higher the initial cell concentration, the longer it takes to lower the survival percentage of DH5α. In a solution with high initial cell concentration, the cells are packed closely and only a small percentage of the cells would be in contact with the TiO_2 film surface. It is not surprising that only a small portion of the cells are killed in the initial stage of irradiation. Moreover, the dead cells cannot diffuse away easily from the film surface and they stayed in contact with the film surface. The chance for the living cells to come in contact with the film surface would be lowered. Therefore, the amount of living cells relative to the dead cells is high for the first 20 min in the high initial cell concentration setup. (Figs. 1a, 2a and 3a) As time goes

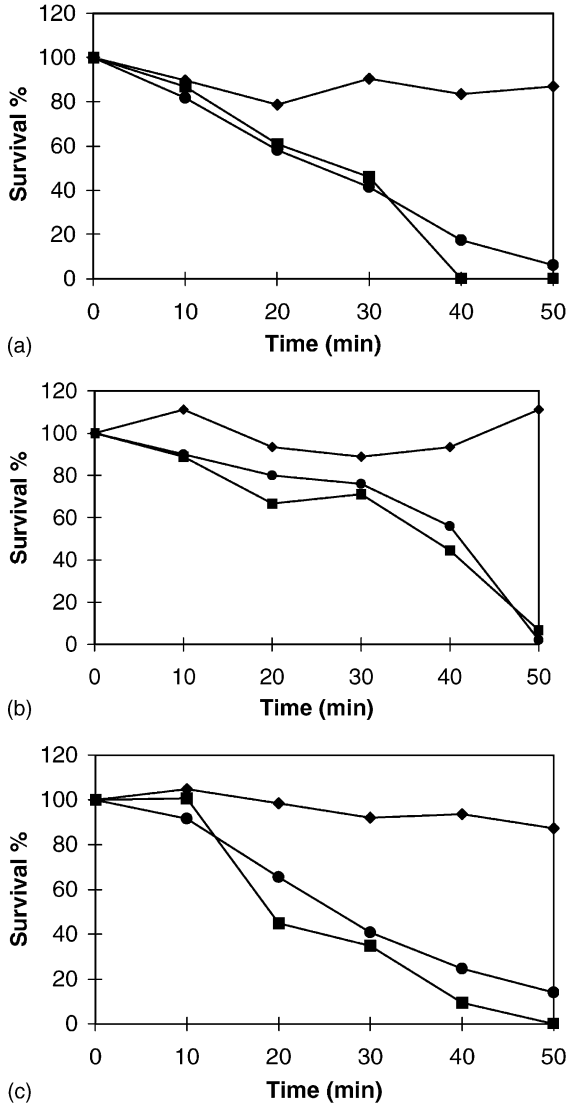

Fig. 2. Effect of SG- and RM-TiO_2 thin films on JM109 survival as a function of time. Initial concentration: (a) 10^6 CFU ml^{-1}; (b) 10^5 CFU ml^{-1}; (c) 10^4 CFU ml^{-1}. Glass (◆); SG-TiO_2 (■); RM-TiO_2 (●).

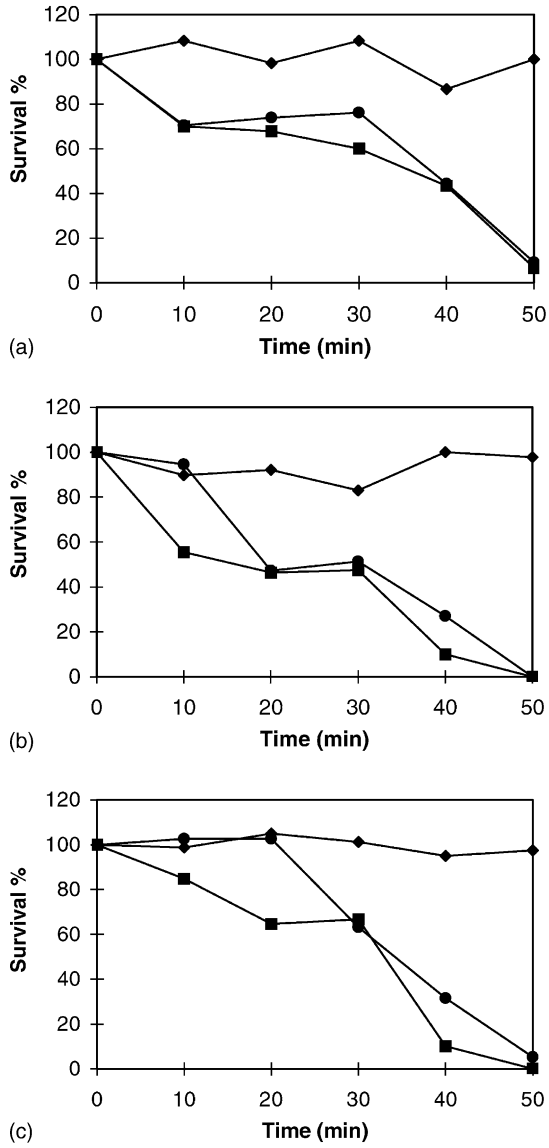

Fig. 3. Effect of SG- and RM-TiO_2 thin films on XL1 Blue MRF' survival as a function of time. Initial concentration: (a) 10^6 CFU ml^{-1}; (b) 10^5 CFU ml^{-1}; (c) 10^4 CFU ml^{-1}. Glass (◆); SG-TiO_2 (■); RM-TiO_2 (●).

on, this shielding effect would decrease gradually. The survival percentage starts to drop at about 40–50 min as more bacterial cells can come in contact with the film surface and be degraded by the oxidizing species.

For lower initial cell concentrations, there are only a limited number of bacterial cells on the film surface. Therefore, the dead cells would not affect the killing of the other living cells, and the survival percentage drops gradually according to the time of UV irradiation [33].

For the strains of *E. coli* JM109 and XL1 Blue MRF' at cell concentrations of 10^4, 10^5 and 10^6 CFU ml^{-1}, the survival percentage of the cells on the two types of TiO_2-coated glass reached near-zero levels after 50 min of UV illumination. For JM109 at cell concentration of 10^6 CFU ml^{-1} (Fig. 2a), the bacterial survival percentage decreased gradually to 80 and 60% after 30 and 40 min of UV illumination, respectively and reached near-zero levels at 50 min. Similar trends were obtained for initial cell concentration of 10^5 CFU ml^{-1} (Fig. 2b) and 10^4 CFU ml^{-1} (Fig. 2c) for JM109. The survival percentage decreased gradually as the time of UV illumination increased, and reached <10% for both of the TiO_2 films at 50 min. For XL1 Blue MRF' at cell concentration of 10^6 CFU ml^{-1} (Fig. 3a), the bacterial survival percentage for the two types of TiO_2 film ranged between 80 and 100% for the first 30 min, which then dropped to 45% at 40 min and finally reached <10% at 50 min of UV irradiation. For initial cell concentrations of 10^5 CFU ml^{-1} (Fig. 3b) and 10^4 CFU ml^{-1} (Fig. 3c) for XL1 Blue MRF', the two types of TiO_2 film exhibited different bactericidal behavior during the initial stage of irradiation. The SG-TiO_2

film lowered the survival percentage of XL1 Blue MRF' by about 45% in the first 10 min while the RM-TiO_2 film only lowered the survival percentage by 10% (Fig. 3b). Also from Fig. 3c, it was observed that SG-TiO_2 film also shows a better bactericidal activity than the RM-TiO_2 film in the first 20 min of UV irradiation. When we studied Fig. 1c again, in the first 10 min of irradiation, RM-TiO_2 film lowered the survival percentage of DH5α by 45% while the SG-TiO_2 film only decreased the survival percentage of DH5α by about 5%. Such a difference in the reactivity of the two types of TiO_2 film towards different strains of *E. coli* may depend on the strain of *E. coli*. However, we cannot give a conclusion in this observation, as we have no data on the different strains of *E. coli* used.

The better overall bactericidal activity for the SG-TiO_2 film towards the photodegradation of JM109 and especially XL1 Blue MRF' can be explained. The SG-TiO_2 film has a stronger absorption for UV light (as shown in Fig. 5), so more oxidizing species can be generated and used to kill the bacterial cells when compared with the RM-TiO_2 film in the initial stage of UV irradiation. In the later stage of irradiation, the dead *E. coli* cells remain on the film surface for both of the TiO_2 films, so that the living bacteria cannot reach the film surface and the difference in bactericidal activities of the two types of film are not prominent.

The size and the shape of the *E. coli* cells of different strains maybe different, which maybe responsible for the different bactericidal behavior observed. For short irradiation times, different strains of *E. coli* may have different extents of tolerance to the oxidizing species generated by the irradiated TiO_2 film. For an *E. coli* cell of larger size and more regular shape, the surface area of the cell in contact with the TiO_2 film would be larger, since photodegradation of the bacterial cells occurs only when the cells are in contact with the TiO_2 film, therefore, a single cell with large surface area in contact with the TiO_2 film surface would be killed in a shorter time, as the chance of the cell being damaged by the oxidizing species would be higher.

3.2. Photocatalytic activity measurement

Oxidation of acetone in the gaseous phase using RM-TiO_2 films was more effective than when using SG-TiO_2 films. Ten pieces of the RM- and the SG-TiO_2 films can degrade 13 and 3 ppm of the acetone in 1 h, respectively.

The results for the degradation of RB in aqueous solution are shown in Fig. 4. Obviously, RB could not be degraded by long wavelength UV irradiation alone. However, with the addition of a piece of TiO_2-coated glass (SG- or RM-TiO_2) while being irradiated under UV light, the concentration started to decrease. The experiment terminated at 40 min of UV irradiation, similar to the time for the bactericidal experiment. Both types of the TiO_2 films displayed similar photodegradation activities toward RB in aqueous solution. The dye concentration decreased by about 30% after 40 min.

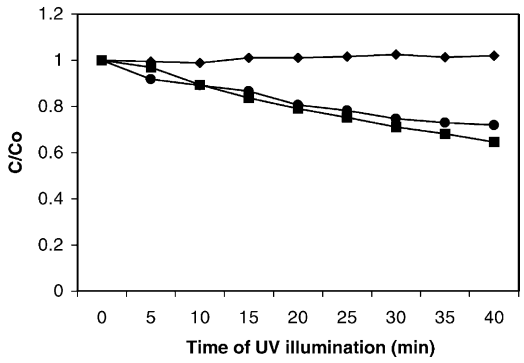

Fig. 4. Photodegradation of RB versus UV irradiation time for the RM- and SG-TiO_2 films. Initial dye concentration is 4×10^{-6} mol dm^{-3}. Without TiO_2 (◆); SG-TiO_2 (■); RM-TiO_2 (●).

The condition for the photodegradation of RB is likely to be similar to that of the bactericidal experiment, since both of them are performed in aqueous solution. The reason why RM-TiO_2 film shows a better photocatalytic activity in the gaseous phase but the aqueous phase is not predictable. The enhanced photocatalytic activity of RM-TiO_2 film is attributed to its increased surface area.

From the AFM results (Fig. 6), the RM-TiO_2 film has a higher root mean square roughness value (R_{rms}) than the SG-TiO_2 film. Hence, the RM-TiO_2 film has a larger surface area than the SG-TiO_2 film.

For the degradation of acetone in the gas phase, as acetone molecules are small enough to diffuse into the porous structure of the RM-TiO_2 film, the larger surface area of the RM-TiO_2 film would give a better photocatalytic activity than the SG-TiO_2 film in the gas phase, especially in the degradation of small organic pollutants. Also, the degraded products are small enough so that they can easily diffuse away from the TiO_2 film surface in the gaseous phase, leaving the new film surface for degrading the remaining acetone molecules. Therefore, the increase of photocatalytic activity of the RM-TiO_2 film is caused by the increase in contact area for acetone with an increase in specific surface area.

For the degradation of RB and the *E. coli* cells in the aqueous phase, the size of a RB molecule is larger than that of acetone while, the size of an *E. coli* cell is even larger in the micron range, so it is not easy for them to diffuse into the porous structure of the RM-TiO_2 film. As a result, the increased surface area of the RM-TiO_2 film does not result in enhanced photocatalytic activity towards the degradation of RB and *E. coli*. Also, when the experiment was performed, the dye solution and the bacterial cell solution were put on the TiO_2-coated glass slide without stirring. Diffusion of the degradation products and the dead cells was not easy in such stationary aqueous phase, so the TiO_2 film surface was not utilized effectively and there was little difference between the two types of TiO_2 film in the degradation of RB and *E. coli* in aqueous phase.

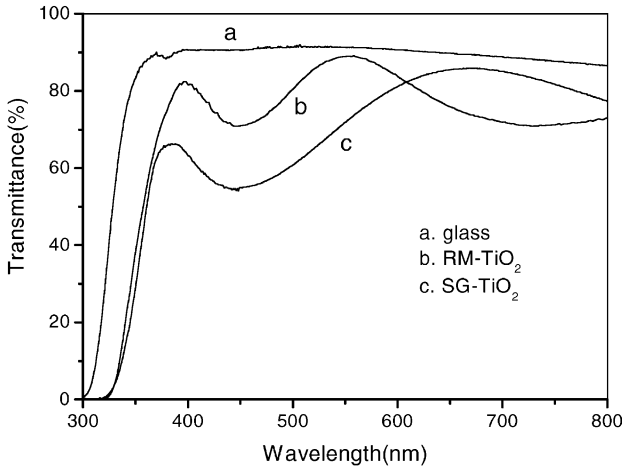

Fig. 5. UV-Vis spectra of glass (a), RM-TiO_2 (b), and SG-TiO_2 (c) films deposited on glass.

3.3. Thickness and transmittance of SG- and RM-TiO_2 thin films

As determined by a surface profiler (Alpha-step 500), the film thicknesses of the SG- and RM-TiO_2 were found to be 0.17 and 0.20 mm, respectively. The two types of TiO_2 thin film prepared by the above methods are optically transparent. Fig. 5 shows the UV-Vis absorption spectra of SG- and RM-TiO_2 films deposited on glass, together with that of a plain glass substrate. The transmittance of glass is about 90% over the visible light spectral region and its absorption edge is at about 330 nm (curve a). The transmission spectra for the SG- and RM-TiO_2 films on glass show some different features.

For the SG-TiO_2 film, the transmittance is about 80% at wavelengths near 800 nm (curve c), and it gradually drops at shorter wavelengths until it reaches its first minimum value of 55% at 450 nm. At even shorter wavelengths, the transmittance rises and reaches about 65% at 380 nm. After that, the transmittance decreases rather quickly, and finally approaches zero at around 320 nm. For the RM-TiO_2 film, the transmittance is about 75% at wavelengths near 650 nm (curve b) and gradually rises at shorter wavelengths until it reaches its first maximum value of 88% at near 550 nm. At shorter wavelengths, the transmittance drops and reaches its minimum value of 70% at 450 nm. After that, the transmittance increases and drops again, and at about 390 nm, it decreases rather quickly, finally approaching zero at around 330 nm. The oscillation of the curve between 380 and 800 nm is due to the interference between the TiO_2 film and the glass substrate [41]. The quick decrease below 380 nm is due to the absorption of light caused by the excitation of electrons from the valence band to the conduction band of TiO_2. The difference in transmittance of the two types of TiO_2 films was attributed to the differences in film thickness and absorption of light.

Compared with the transmission spectrum of SG-TiO_2 films, the absorption edge of RM-TiO_2 films is observed at a shorter wavelength range. RM-TiO_2 films consist of relatively small crystallites that show a pseudo-"blue shift" [41–46]. As a result, the band gap of RM-TiO_2 would increase; hence the oxidizing power of RM-TiO_2 is greater than that of SG-TiO_2. The bactericidal activity of RM-TiO_2 films should be higher than that of SG-TiO_2 films. However there is a second factor to be considered. The UV light source in this study has an emission maximum at 365 nm, at which the SG-TiO_2 exhibits a stronger absorption. The effects of blue shift and UV absorption offset each other resulting in two TiO_2 films with similar bactericidal activities.

3.4. Surface morphologies and roughness of thin films

The surface morphologies and roughness of SG- and RM-TiO_2 films are obviously different. Fig. 6a–d shows the two- and three-dimensional AFM images of these films. From Fig. 6a and b, it can be seen that the SG-TiO_2 thin film has a granular microstructure and is composed of spherical particles of about 80 nm in diameter. The porous structure between the TiO_2 particles is not clearly seen in SG-TiO_2 film. Fig. 6c and d show that RM-TiO_2 film is composed of monodispersed spherical particles of about 15 nm in diameter and that there is a mesoporous structure between the monodispersed TiO_2 particles [37]. Monodispersity is an advantage of the reverse micellar route for synthesizing TiO_2 nanoparticles by hydrolysis of titanium isopropoxide [37,38]. There is competition for water molecules between the hydrolysis process and the hydration of surfactant polar heads. Growth limitations and uniform sized particle formation can be obtained by restructuring the surfactant molecules around the polar species formed during hydrolysis [38]. In addition to particle diameter, AFM image analysis also gives the value of surface roughness. The R_{rms} of SG- and RM-TiO_2 are 0.638 and 1.054 nm, respectively. These show that the RM-TiO_2 film is rougher than the SG-TiO_2 film.

Since RM-TiO_2 film is rougher and has a larger surface area for absorbing UV radiation, it can compensate for the lower light intensity that can be utilized as the UV light source has an emission maximum at 365 nm. Therefore, it is not surprising that even though the RM-TiO_2 film has a larger surface area, its bactericidal activity and photocatalytic activity for degradation of RB in aqueous solution is similar to that of the SG-TiO_2 film. Moreover, the small acetone molecules can diffuse into the porous structure of the RM-TiO_2 film so the larger surface area of the RM-TiO_2 film is beneficial for the degradation of acetone in the gaseous phase and hence it shows better photocatalytic activity when compared with the SG-TiO_2 film. Since the RB molecules and the *E. coli* cells are too large for rapid diffusion into the porous structure of RM-TiO_2 film, the increased surface area in the pores cannot be used to give enhanced photocatalytic

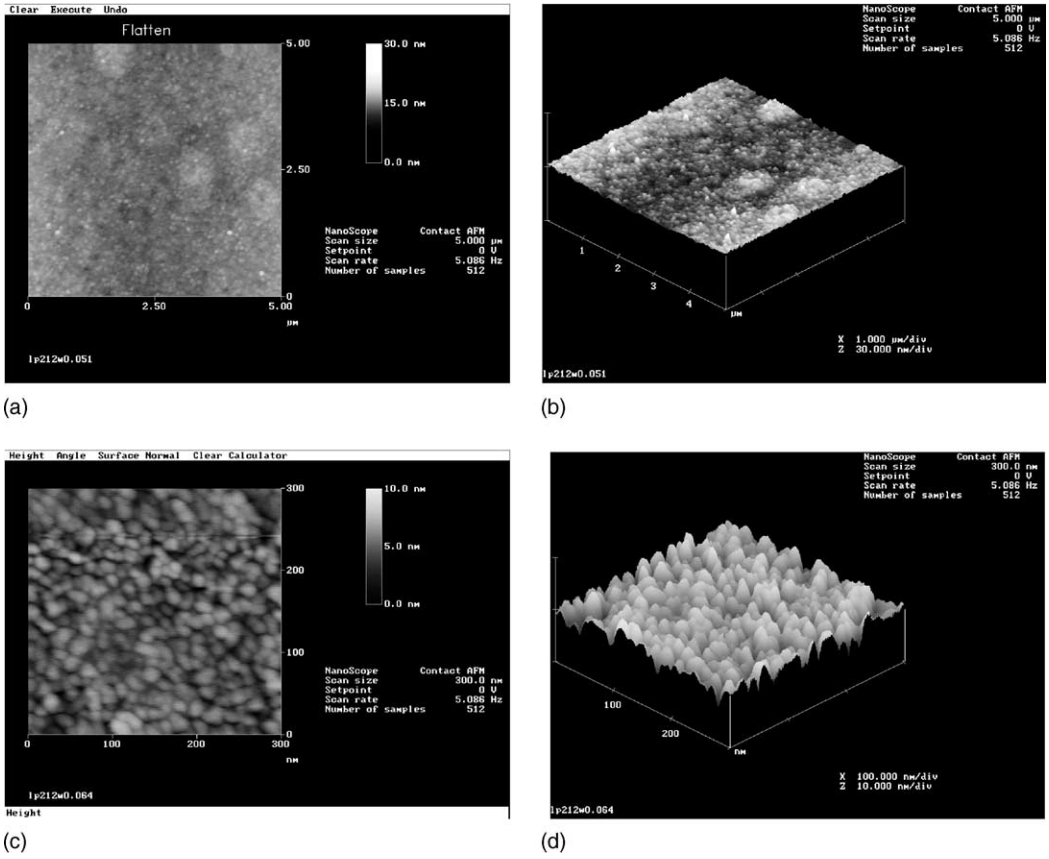

Fig. 6. AFM two- and three-dimensional images of the SG-TiO_2 (a) and (b), and RM-TiO_2 (c) and (d) thin films deposited on glass.

activities as the photodegradation process occurs only when the substrates are in contact with the TiO_2 film surface.

3.5. Crystalline phase and crystallite size of thin films

The XRD patterns of the SG- and RM-TiO_2 films deposited on glass are shown in Fig. 7. The peaks appear more intense for the SG-TiO_2 film, which means its crystalline size is larger than that of the RM-TiO_2. The average crystallite sizes of the SG- and RM-TiO_2 films were 7.2 and 5.7 nm, respectively, as measured by the line broadening method and the Scherrer equation. These values are much smaller than that obtained from AFM measurements because AFM tends to show the overall aggregates rather than individual particles. In addition, the width at the half height of the main peak of anatase structure of SG-TiO_2 film is narrower than that of the RM-TiO_2 film. This indicates the formation of larger crystallites in the SG-TiO_2 films. The apparent "blue shift" in the spectrum of the RM-TiO_2 sample also confirms the presence of smaller crystallites in RM-TiO_2 films.

3.6. XPS studies

Fig. 8 shows the XPS survey spectra of the RM-TiO_2 (a), and SG-TiO_2 (b) thin films. It can be seen that both of the TiO_2 thin films contain the elements Ti, O, C and Na. The photoelectron peak for Ti 2p appears clearly at binding energy E_b = 458 eV, O 1s at E_b = 530 eV, C 1s at E_b = 285 eV, Na 1s at E_b = 1072 eV and Na KLL at E_b = 496 eV. The Na peak observed in both of the spectra of the TiO_2

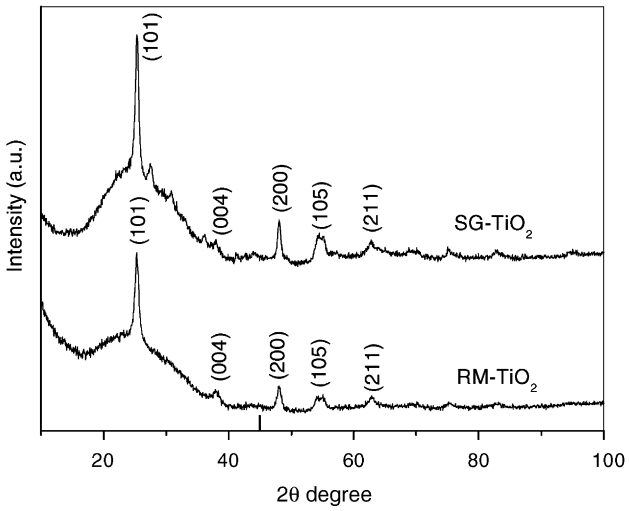

Fig. 7. XRD patterns of TiO_2 thin films deposited on glass—the thickness of the SG- and RM-TiO_2 thin films are 0.17 and 0.20 mm, respectively.

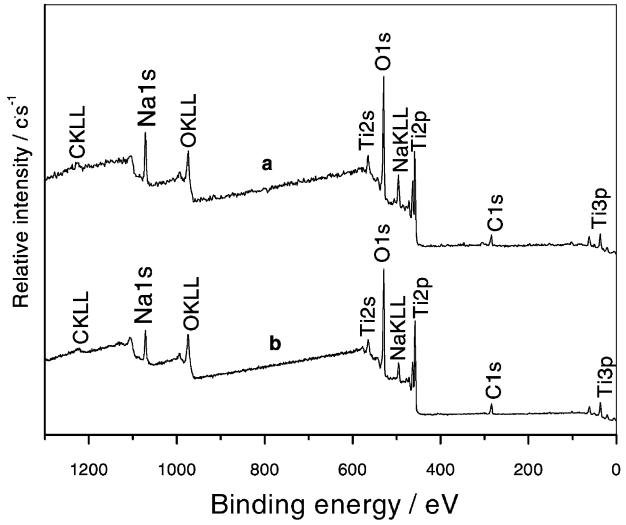

Fig. 8. XPS survey spectra for RM-TiO_2 (a), and SG-TiO_2 (b) thin films.

thin films implies that sodium ions migrate from the glass substrates into the film and that some chemical reactions might occur at the interface between the films and the glass substrates [35,47,48]. As shown in Table 1, the amounts of sodium on the surface of the film as measured by XPS are 14.4 and 8.5 at.% for RM- and SG-TiO_2 samples, respectively. The incorporation of Na could account for the less crystallized state of titanium dioxide when it is deposited on glass [35,49,50]. The element C in Fig. 8 is attributed to the residual carbon from precursor solution and the adventitious hydrocarbon from the XPS instrument itself. The C content in Table 1 originates solely from the residual carbon such as unhydrolyzed alkoxide groups, carbonate and so on and excludes the adventitious hydrocarbon from specimen handling or pumping oil [51].

Fig. 9 shows the high-resolution XPS spectra of the O 1s region for RM-TiO_2 (a), and SG-TiO_2 (b) thin films. The O ls region is composed of two peaks. The main peak is attributed to Ti–O in TiO_2 while the minor peak is attributed to the hydroxyl group. Table 2 lists the results of curve fitting of XPS spectra for the two TiO_2 samples, where r_i (%) shows the ratio of each contribution to the total of both kinds of oxygen contributions. As seen in Table 2 and Fig. 8, the hydroxyl content of the RM-TiO_2 sample is only slightly higher than that of the SG-TiO_2 sample. Usually, the hydroxyl content on the surface of TiO_2 films is related to the photocatalytic activity [47,52], therefore, we would expect

Table 1
Composition (at.%) of RM- and SG-TiO_2 thin films according to XPS analysis

Films	Ti	O	C	Na
RM-TiO_2	20.4	51.6	9.6	14.4
SG-TiO_2	21.6	51.8	14.9	8.5

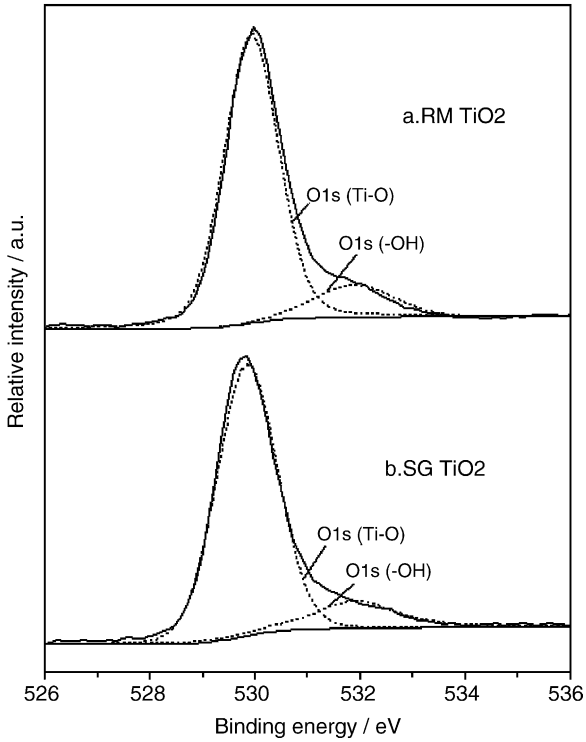

Fig. 9. High-resolution XPS spectra of the O 1s region for the RM-TiO_2 (a), and SG-TiO_2 (b) thin films.

Table 2
Results of curve-fitting of the high-resolution XPS spectra for the O 1s region

Film	E_b (eV)	r_i (%)
RM-TiO_2		
O 1s (Ti–O)	529.90	83.3
O 1s (OH)	531.90	16.7
SG-TiO_2		
O 1s (Ti–O)	529.85	84.9
O 1s (OH)	531.90	15.1

the SG- and RM-TiO_2 thin films to display similar bactericidal activities.

4. Conclusions

Two types of TiO_2 thin films were prepared and tested. Both SG- and RM-TiO_2 thin films show significant bactericidal activity under UV irradiation. These films can kill the *E. coli* DH5α, JM109 and XL1 Blue MRF' effectively. The RM-TiO_2 film shows a better overall bactericidal activity towards DH5α than the SG-TiO_2 film, while SG-TiO_2 film is more effective towards JM109 and XL1 Blue MRF'. Results indicate that photocatalytically induced bactericidal effect is related to the physical properties of the strains, including the size and shape of bacterial cells. Dependency on

the initial *E. coli* concentration has also been observed. In general, the higher the initial cell concentration, the longer it takes to lower the survival percentage of *E. coli*.

The RM-TiO_2 film displays higher photocatalytic activity than that of the SG-TiO_2 film in the gaseous phase degradation of acetone. This is because the molecular size of acetone is small enough to diffuse into the porous structure of the RM-TiO_2 film. The increased surface area of the RM-TiO_2 film can be utilized effectively providing an enhancement in photocatalytic activity when compared with the SG-TiO_2 film. However, their photocatalytic activities as measured by the aqueous phase degradation of RB and *E. coli* are about the same. This is because the molecular size of RB and *E. coli* cells are too large for easy diffusion into the porous structure of the RM-TiO_2 film. Therefore, the increased surface area of the RM-TiO_2 film would not be beneficial in the degradation of large molecules/species.

Acknowledgements

The work described in this paper was partially supported by a grant from the National Natural Science Foundation of China, and Research Grants Council of the Hong Kong Special Administrative Region, China (project no. N_CUHK 433/00).

References

[1] R. Sommer, M. Lhotsky, T. Haider, A. Cabaj, J. Food Protect. 63 (2000) 1015.
[2] A. Fujishima, K. Honda, Nature 283 (1972) 37.
[3] R.M. Alverici, W.F. Jardim, Appl. Catal. 14 (1997) 55.
[4] K.H. Wang, H.H. Tsai, Y.H. Hsieh, Chemosphere 36 (1998) 2763.
[5] C.H. Hung, B.J. Marinas, Environ. Sci. Technol. 31 (1997) 562.
[6] C.H. Hung, B.J. Marinas, Environ. Sci. Technol. 31 (1997) 1440.
[7] W.A. Jacoby, M.R. Nimlos, D.M. Blake, Environ. Sci. Technol. 28 (1994) 1661.
[8] S. Yamazaki-Nishida, X. Fu, M.A. Anderson, K. Hori, J. Photochem. Photobiol. 97 (1996) 175.
[9] M.R. Nimlos, W.A. Jacoby, D.M. Blake, T.A. Milne, Environ. Sci. Technol. 27 (1993) 732.
[10] H. Einaga, S. Futamura, T. Ibusuki, Phys. Chem. Chem. Phys. 1 (1999) 4903.
[11] W.F. Jardim, S.G. Moraes, M.M.K. Takiyama, Water Res. 31 (1997) 1728.
[12] M.L. Sauer, M.A. Hale, D.F. Ollis, J. Photochem. Photobiol. 88 (1995) 169.
[13] P. Boarini, V. Carassiti, A. Maldotti, R. Amadelli, Langmuir 14 (1998) 2080.
[14] M.M. Ameen, G.B. Raupp, J. Catal. 184 (1999) 112.
[15] A.J. Bard, J. Phys. Chem. 86 (1982) 172.
[16] O.C. Zafiriou, Environ. Sci. Technol. 18 (1984) 358.
[17] L.P. Childs, D.F. Ollis, J. Catal. 66 (1980) 383.
[18] D.F. Ollis, Environ. Sci. Technol. 19 (1985) 480.
[19] N. Serpone, Solar Energy Mater. Solar Cells 38 (1995) 369.
[20] T. Matsunaga, R. Tomoda, T. Nakajima, H. Wake, FEMS Microbiol. Lett. 29 (1985) 211.
[21] T. Matsunaga, R. Tomoda, T. Nakajima, N. Nakamura, T. Komine, Appl. Environ. Microbiol. 54 (1988) 1330.
[22] C. Wei, W.-Y. Lin, Z. Zainai, N.E. Williams, K. Zhu, A.P. Kruzic, R.L. Smith, K. Rajeshwar, Environ. Sci. Technol. 28 (1994) 934.
[23] R.J. Watts, S. Kong, M.P. Orr, G.C. Miller, B.E. Henry, Water Res. 29 (1995) 95.
[24] M. Bekbolet, C.V. Araz, Chemosphere 32 (1996) 959.
[25] M. Stevenson, K. Bullock, W.-Y. Lin, K. Rajeshwar, Res. Chem. Intermed. 23 (1997) 311.
[26] M. Bekbolet, Water Sci. Tech. 35 (1997) 95.
[27] P.-C. Maness, S. Smolinski, D.M. Blake, Z. Huang, E.J. Wolfrum, W.A. Jacoby, Appl. Environ. Microbiol. 65 (1999) 4094.
[28] J.A. Herrera Melian, J.M. Dona Rodriguez, A. Viera Suarez, E. Tello Rendon, C. Valdes do Campo, J. Arana, J. Perez Pena, Chemosphere 41 (2000) 323.
[29] A.G. Rincon, C. Pulgarin, N. Adler, P. Peringer, J. Photochem. Photobiol. 139 (2001) 233.
[30] T. Matsunaga, M. Okochi, Environ. Sci. Technol. 29 (1995) 501.
[31] I.M. Butterfield, P.A. Christensen, T.P. Curtis, J. Cunlazuardi, Water Res. 31 (1997) 675.
[32] K. Sunada, Y. Kikuchi, K. Hashimoto, A. Fujishima, Environ. Sci. Technol. 32 (1998) 726.
[33] W.A. Jacoby, P.C. Maness, E.J. Wolfrum, D.M. Blake, J.A. Fennell, Environ. Sci. Technol. 32 (1998) 2650.
[34] Y.-S. Choi, B.-W. Kim, J. Chem. Technol. Biotechnol. 75 (2000) 1145.
[35] J.G. Yu, X.J. Zhao, Mater. Res. Bull. 35 (2000) 1293.
[36] A. Fujishima, T.N. Rao, D.A. Tryk, J. Photochem. Photobiol. 1 (2000) 1.
[37] E. Stathatos, P. Lianos, F. DelMonte, D. Levy, D. Tsiourcas, Langmuir 13 (1997) 4295.
[38] E. Stathatos, P. Lianos, Langmuir 16 (2000) 2398.
[39] J.C. Yu, J.G. Yu, J.C. Zhao, Appl. Catal. 36 (2002) 31.
[40] J.G. Peak, M.J. Peak, Photochem. Photobiol. 36 (1982) 103.
[41] T. Yoko, K. Kamiya, S. Sakka, Yogyo Kyokai Shi 95 (1985) 12.
[42] A.L. Linsebigler, G. Lu, J.T. Yates Jr., Chem. Rev. 95 (1995) 735.
[43] J.G. Yu, X.J. Zhao, Q.N. Zhao, J. Mater. Sci. Lett. 19 (2000) 1015.
[44] K. Kato, A. Tsuzuki, H. Taoda, Y. Torii, T. Kato, Y. Butsugan, J. Mater. Sci. 295 (1994) 5911.
[45] M. Anpo, T. Shima, S. Kodama, Y. Kubokawa, J. Phys. Chem. 91 (1987) 4305.
[46] D. Duonghong, E. Borgarello, M. Gratzel, J. Am. Chem. Soc. 103 (1981) 4685.
[47] J.G. Yu, X.J. Zhao, Mater. Res. Bull. 36 (2001) 97.
[48] A. Fernandez, G. Lassaletta, V.M. Jimenez, A. Justo, A.R. Gonzalez-Elipe, J.M. Herrmann, H. Tahiri, Y. Ait-Ichou, Appl. Catal. 7 (1995) 49.
[49] Y. Paz, Z. Luo, L. Rabenberg, A. Heller, J. Mater. Res. 10 (1995) 2842.
[50] Y. Paz, A. Heller, J. Mater. Res. 12 (1997) 2759.
[51] C. Wagner, G. Muilnberg, Handbook of X-ray Photoelectron Spectroscopy, Physical Electronics Division, Perkin-Elmer Corporation, Eden Prairie, MN, 1979.
[52] M.R. Hoffmann, S.T. Martin, W. Choi, D.W. Bahnemann, Chem. Rev. 95 (1995) 69.